# Zero-Forcing Electrical Filters for Direct Detection Optical Systems

Peter C. Li, *Member, IEEE*, and Pierre A. Humblet, *Fellow, IEEE*

*Abstract*— **Intersymbol interference (ISI) in direct detection optical systems can limit channel spacing in frequency division multiplexing systems, and data rates, and transmission distances in long-haul transmission. It is desirable to reduce or cancel ISI in these situations. We investigate zero-forcing electrical filters to cancel ISI, and obtain tight performance bounds for minimum noise variance zero-forcing filters.**

**We apply the results to Mach–Zehnder and Fabry–Perot filters, and to fibers with second order dispersion. We compare the performance of zero-forcing filters to that of rectangular impulse response filters and find that zero-forcing filters are advantageous in severe ISI situations with multilevel signaling.**

## I. Introduction

We consider direct detection optical systems where the receiver front-end is composed of an optical filter, a photodetector, and a low-pass electrical filter. In frequency division multiplexing systems, an optical demultiplexing filter is placed before the photodetector to select the desired signal. When the channel spacing gets small, the filter bandwidth needs to be narrow. This introduces intersymbol interference (ISI) for the desired signal. This distortion can limit the spacing of channels and prevent multilevel signaling. In long distance transmission, the fiber itself plays the role of an optical filter as it disperses the transmitted pulse. The dispersion of the fiber causes ISI by broadening the transmitted pulse.

The nonlinearity of the photodiode makes the ISI problem that we consider nonclassical [1], [2]. Other signal processing approaches to receiver designs and techniques to reduce ISI are presented in [2]–[5]. The originality of this work is that we present a framework to study optical ISI in direct detection systems and to design optimal filters from basic principles. Optical domain techniques can also be utilized, see [6] and [7] and the references therein. They can complement our approach.

Based on the model presented in Section II, we consider in Section III the post-detection signal space. It plays an important role in Section IV, where we design zero-forcing receivers. In Section V, we consider applications in frequency division multiplexing systems, and long-haul systems. Receiver structures constructed using the least mean square criterion are presented in [8] while those for decision feedback and maximum likelihood are presented in [9].

Paper approved by L. Kazovsky, the Editor of Optical Communications of the IEEE Communications Society. Manuscript received January 15, 1995; revised August 2, 1995. This work was supported by the National Science Foundation under Grant NCR-9206379.

P. C. Li is with the Naval Undersea Warfare Center, Newport, RI 02841–1708 USA.

P. A. Humblet is with Eurecom, Sophia Antipolis, 06904 France.

Publisher Item Identifier S 0090-6778(96)04350-4.

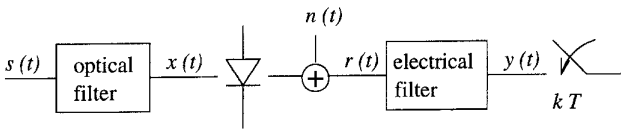


Fig. 1. The receiver front-end includes an optical filter, a photodiode and a low-pass electrical filter followed by a sampler.

## II. Model

In our model, a chirp-free transmitter sends pulse modulated signals to a receiver. The transmitted signal can be written as

$$s(t) = \sqrt{2}\,\mathrm{Re}\left\{ \sum_{k=-\infty}^{\infty} a_k g(t - kT) e^{j2\pi f_c t} \right\} \tag{1}$$

where $g(t)$ is the complex envelope of the transmitted pulse. The $k$th transmitted amplitude is $a_k$. The carrier frequency is $f_c$, and the baud rate is $1/T$. Although we deal with direct detection, phase variations can be helpful in some cases. This is discussed in the Appendix. For now, we assume the $a_i$'s are real. In particular, we consider the following set of transmitted amplitudes

$$a_k \in \left\{ \sqrt{\frac{i}{M-1}} \,\middle|\, 0 \le i \le M-1 \right\} \tag{2}$$

where $M$ is the number of signaling levels. The square root in (2) allows the post-detection product amplitude, $a_k^2$, to be evenly spaced. The factor $M-1$ in the denominator normalizes the peak amplitude to one and the mean square to 1/2.

When comparing different $M$-ary signaling sets, we keep the bit rate fixed. The transmitted symbols are sent at a slower rate, compared to the two level case, so we elongate the transmitted pulse in time by a factor of $\log_2 M$. It follows from the above assumptions that the peak and average transmitted power are independent of $M$ when the transmitted pulses do not overlap in time. Under the same assumptions, the average energy per bit is also independent of $M$.

The transmitted signal is passed through an optical filter that models either a dispersive fiber-optic channel for long-haul transmission or an optical demultiplexing filter for frequency division multiplexing systems. In Fig. 1, we show the optical filter followed by a photodetector and a low-pass electrical filter. This shows the receiver front-end where the optical signal is converted to an electrical signal.

We write the received signal after the optical filter as

$$x(t) = \sqrt{2}\,\mathrm{Re}\left\{ \sum_{k=-\infty}^{\infty} a_k p(t-kT) e^{j2\pi f_c t} \right\} \tag{3}$$

where $p(t)$ is the complex envelope of the received pulse taking into account the transmitted pulse and the channel response.

The photodetector is modeled as a square-law device whose output is proportional to the magnitude square of the received signal envelope. The post-detection received signal, $r(t)$, can be written as

$$r(t) = \sum_{i,j=-\infty}^{\infty} a_i a_j p(t-iT) p^*(t-jT) + n(t) \tag{4}$$

where * denotes the complex conjugate. The thermal noise, $n(t)$, is assumed to be the dominant source of noise, modeled as additive white Gaussian noise. Since the left hand side of (4) is real, we can take the real part of the right hand side. We can rewrite (4) as

$$r(t) = \sum_{i,j=-\infty}^{\infty} a_i a_j p_{i,j}(t) + n(t) \tag{5}$$

where $p_{i,j}(t) = \mathrm{Re}\{p(t-iT)p^*(t-jT)\}$. We refer to the $p_{i,j}(t)$'s as product waveforms.

## III. Signal Space

The signal spaces that we consider in designing the zero-forcing filters are the following. We let the desired signal be $a_0^2 p_{0,0}(t)$ in (4) and we consider the other $a_i a_j p_{i,j}(t)$'s as ISI waveforms. The *ISI space*, $I$, is the space spanned by $p_{i,j}(t)$'s without $p_{0,0}(t)$, and the *signal space* is the space spanned by $I$ and $p_{0,0}(t)$.

We can describe the set of product waveforms in a more convenient manner by using the following:

$$p_{i,j}(t) = p_{j,i}(t). \tag{6}$$

From this property, we need only consider the following subset of product waveforms:

$$\{p_{i,j}(t) \mid i \geq j\}. \tag{7}$$

These product waveforms are also related in that one product waveform can be written as another product waveform shifted in time, i.e., another way of expressing the above set of product waveforms is to consider the following:

$$p_{i,j}(t) = p_{0,j-i}(t-iT). \tag{8}$$

Let $k = j - i$. Making this substitution in (8), we can rewrite (7) as

$$\{p_{0,k}(t-iT) \mid k \leq 0 \quad \text{and} \quad -\infty < i < \infty\}. \tag{9}$$

### A. Dimension of the Signal Space Per Baud

In defining the dimension of the signal space per baud, we consider the following signal space. We have a finite set of transmitted amplitudes, $a_1, \ldots, a_n$, and the other amplitudes set to zero. Then the electrical signal is a weighted sum of product waveforms in

$$\{p_{i,j}(t) \mid 1 \leq i \leq n \quad \text{and} \quad 1 \leq j \leq n\}. \tag{10}$$

The signal space composed of product waveforms in (10) has a finite dimension, say $d_n$. We define the dimension of the signal space per baud as $\mathcal{D} = \limsup_{n\to\infty} d_n/n$. When the duration of the complex envelope of the received pulse $p(t)$ is finite, $\mathcal{D}$ is finite. The converse does not hold, i.e., later we will see in Section V a case where $\mathcal{D}$ is finite but the duration of $p(t)$ is infinite.

### B. An Approximation to the Signal Space

For numerical computation, we want to be able to make an approximation to the signal space by removing waveforms whose energies are relatively small. From (9), we see that the product waveforms $p_{i,j}(t)$'s are time-translated versions of $p_{0,j}(t)$'s for $j \leq 0$. For our approximation, we only consider $p_{i,j}(t)$'s that are time translations of $p_{0,j}(t)$'s for $-k' \leq j \leq 0$. The value of $k'$ is determined as follows. Let

$$\mathcal{L} = \sum_{i=0}^{\infty} \langle p_{0,-i}, p_{0,-i} \rangle \tag{11}$$

be the sum of the energy of $p_{0,-i}(t)$'s such that $i \geq 0$. Let $k'$ be the smallest positive integer such that

$$\gamma \cdot \mathcal{L} \leq \sum_{i=0}^{k'} \langle p_{0,-i}, p_{0,-i} \rangle \tag{12}$$

where $\gamma$ is a fraction between zero and one. Let $\tilde{S}_{(\gamma)}$ be the signal space for the remaining set of waveforms when $k'$ is a lower bound to $k$ in (9). For example, $\tilde{S}_{(0.90)}$ is the signal space when $\gamma = 0.90$.

### C. Intersymbol Interference

An interference free signal would be

$$r(t) = \sum_i a_i^2 p_{i,i}(t) + n(t) \tag{13}$$

and we will see in the next section how that goal can be achieved. However, we note that ISI can be helpful in the case of binary on–off modulation when the $p_{i,j}(t)$'s are nonnegative and concentrated around $t = iT$, which happens in some applications. There is then little interference with off signals, because $a_i = 0$ in the crossterms of (5), and the interference with on signals is constructive. However, the nonnegativity of the $p_{i,j}(t)$'s offers no advantages when $M > 2$.

## IV. Zero-Forcing Filters

In Section IV-A, we introduce the normalized eye opening as our performance parameter. In designing the zero-forcing filters, we first specify the zero-forcing conditions in the time domain and in the frequency domain. These conditions are presented in Sections IV-B and IV-C. Then we consider approaches to construct zero-forcing filters that minimize the noise variance in Section IV-D.

### A. Normalized Eye Opening

We refer to the vertical openings of a noiseless eye diagram at the sampling time as "eye openings." There are $M-1$ eye openings for $M$-ary signaling. We call the smallest eye opening the *normalized eye opening*, $\xi$, when the electrical filter is normalized to have unit energy. For a zero-forcing filter with amplitude set (2), the eye openings have equal magnitudes and

$$\text{symbol error rate} = \frac{2(M-1)}{M} Q\left(\frac{\xi}{\sqrt{2N_o}}\right) \tag{14}$$

where $Q(x) = \frac{1}{2\pi}\int_x^\infty e^{-\frac{y^2}{2}} dy$ and $N_o/2$ is the spectral density of the additive white Gaussian noise [1]. We assume that the decision thresholds are set at mid-points of eye openings and the transmitted symbols are equally likely.

### B. Time Domain Zero-Forcing Conditions

For the time domain and frequency domain conditions, we assume the transmitted amplitude set is stationary. We can consider the zero-forcing conditions for time $t$ =0 without loss in generality. From (5), we write the output of the electrical filter at time $t$ =0 as

$$y(0) = \sum_{i,j} a_i a_j \int p_{i,j}(\sigma) h(\sigma) d\sigma + N \tag{15}$$

where $h(t)$ is the *time-reversed* impulse response of the electrical filter and $N$ is the noise at the sampled output. We can also write the integral $\int p_{i,j}(t)h(t)dt$ as an inner product $\langle p_{i,j}, h\rangle$.

Let the sampled output be the noiseless part of the electrical filter output at time $t$ =0. A filter $h(t)$ is a zero-forcing filter if the sampled output has no ISI, i.e., we want the sampled output to depend only on $a_0^2$. When zero is a possible transmitted amplitude, the necessary and sufficient condition for $h(t)$ to be a zero-forcing filter is

$$\langle p_{0,0}, h\rangle \neq 0, \quad \text{and} \quad \langle p_{i,j}, h\rangle = 0, \quad \text{for } i \neq 0 \quad \text{or} \quad j \neq 0. \tag{16}$$

If this condition is satisfied, the sampled output depends only on the $a_0^2$ term so there is no ISI. To show the necessary part, note first that for a single symbol transmission at time $t = iT$, the sampled output is $a_i a_i \langle p_{i,i}, h\rangle$. Hence, it is necessary that $\langle p_{i,i}, h\rangle == 0$ for $i \neq 0$. For two symbol transmissions at $t = iT$ and $t = jT$, the sampled output is $a_i a_i \langle p_{i,i}, h\rangle + 2a_i a_j \langle p_{i,j}, h\rangle + a_j a_j \langle p_{j,j}, h\rangle$. Apply the necessary condition of the single symbol case. Then, it is necessary for $\langle p_{i,j}, h\rangle = 0$ when $i \neq 0$ or $j \neq 0$.

In [9], the necessary and sufficient conditions for zero-forcing are presented when zero is not a possible transmitted amplitude. Condition (16) applies to systems where there is a nonzero component of $|p(t)|^2$ orthogonal to the ISI space.

### C. Frequency Domain Zero-Forcing Conditions

We can rewrite (16) as

$$\int \mathrm{Re}\{p(t-nT)p^*(t-mT)\}h(t)dt = \begin{cases} K, & \text{if } n=m=0 \\ 0, & \text{otherwise} \end{cases} \tag{17}$$

where $K \neq 0$. Equivalently, we can write

$$\sum_{n,m} \langle p_{n,m}, h\rangle \delta(t_1 - nT)\delta(t_2 - mT) = K\delta(t_1)\delta(t_2) \tag{18}$$

where $\delta(t)$ is the Dirac delta function. Taking the two dimensional Fourier transform, we can express the above equation as

$$\frac{1}{2T^2}\sum_{n,m}\left[P\left(f_1 - \frac{n}{T}\right)P^*\left(-f_2 + \frac{m}{T}\right) + P^*\left(-f_1 + \frac{n}{T}\right)P\left(f_2 - \frac{m}{T}\right)\right] \cdot H\left(f_1 + f_2 - \frac{n+m}{T}\right) = K \tag{19}$$

for all $f_1$ and $f_2$. $P(f)$ and $H(f)$ are the Fourier transforms of $p(t)$ and $h(-t)$, respectively. This is a generalized Nyquist's criterion in the frequency domain.

When $p(t)$ is real, (19) reduces to

$$\frac{1}{T^2}\sum_{n,m} P\left(f_1 - \frac{n}{T}\right)P\left(f_2 - \frac{m}{T}\right)H\left(f_1 + f_2 - \frac{n+m}{T}\right) = K. \tag{20}$$

It follows from (19) and (20) that the minimum bandwidth for a pulse that can satisfy the zero-forcing condition is $\frac{1}{2T}$; this is the same as the classical linear channel case.

### D. Minimum Noise Variance Zero-Forcing Filters

Among the filters that satisfy the zero-forcing condition (16), we are interested in the one that minimizes the noise variance when $\langle p_{0,0}, h\rangle$ is set equal to a constant; we will refer to this filter as the optimal zero-forcing filter. For the amplitude set that we consider, the optimal zero-forcing filter also maximizes the normalized eye opening.

Note that the time-reversed impulse response of the electrical filter, $h(t)$, can be decomposed into a component in the signal space and a component orthogonal to the signal space. Since we are interested in minimizing the noise variance, we set the orthogonal component to zero, leaving the signal space as the relevant space to consider in designing the filter. Within the signal space, we want $h(t)$ to be proportional to the component of $p_{0,0}(t)$ orthogonal to $I$. This is similar to the approach in [10].

The normalized eye opening of the zero-forcing filter that minimizes the noise variance may be difficult to evaluate

analytically. We can, however, determine upper and lower bounds in Sections IV-D1 and IV-D2, respectively.

*1) Upper Bound:* For the upper bound, we consider a finite set of transmitted amplitudes, $a_{-l} \cdots a_l$, with the other amplitudes set to zero. The signal space involving these amplitudes is a finite dimensional space, which we call $S_l$. Let $I_l$ be the corresponding ISI space generated by product waveforms $p_{i,j}(t) \in S_l$ excluding the waveform $p_{0,0}(t)$. Let $\phi_1(t), \ldots, \phi_n(t)$ be orthonormal waveforms that span $I_l$. Let $h_l(t)$ be the component of $p_{0,0}(t)$ orthogonal to the $\phi(t)$'s and normalized to have unit energy. This waveform is also the additional waveform needed to form a set of orthonormal waveforms $h_l(t), \phi_1(t), \ldots, \phi_n(t)$ that span the space $S_l$. For the amplitude set that we consider, the eye openings are the same. In particular, we can write the normalized eye opening as $\frac{1}{M-1}\langle p_{0,0}, h_l\rangle$ for the signal space $S_l$. We can compute $\langle p_{0,0}, h_l\rangle$ as follows:

$$p_{0,0}(t) = \langle p_{0,0}, h_l\rangle h_l(t) + \sum_{i=1}^{n} \langle p_{0,0}, \phi_i\rangle \phi_i(t) \quad (21)$$

$$\langle p_{0,0}, p_{0,0}\rangle = \langle p_{0,0}, h_l\rangle^2 + \sum_{i=1}^{n} \langle p_{0,0}, \phi_i\rangle^2 \quad (22)$$

and

$$\langle p_{0,0}, h_l\rangle = \sqrt{\langle p_{0,0}, p_{0,0}\rangle - \sum_{i=1}^{n} \langle p_{0,0}, \phi_i\rangle^2}. \quad (23)$$

As we add more ISI waveforms, $\langle p_{0,0}, h_l\rangle$ decreases monotonically because there are additional interference signals and additional $\phi_i(t)$'s being added to (23). Thus, $\frac{1}{M-1}\langle p_{0,0}, h_l\rangle$ is an upper bound to the infinite sequence case.

Note that $h_l(t)$ is not a zero-forcing filter for the infinite sequence case as it was generated from a finite set of transmitted amplitudes. Note also that when l=0, there is no ISI waveform involved and we get the *matched filter bound*, $\frac{1}{M-1}\sqrt{\langle p_{00}, p_{00}\rangle}$.

*2) Lower Bound:* In this construction, we restrict the electrical filter response to the interval $[uT, vT]$. Let $h_{[u,v]}(t)$ denote this filter. The filter output is

$$\underbrace{a_0 a_0 \langle p'_{0,0}, h_{[u,v]}\rangle}_{\text{signal}} + \underbrace{\sum_{p_{i,j}\in I} a_i a_j \langle p'_{i,j}, h_{[u,v]}\rangle}_{\text{ISI}} + \underbrace{N}_{\text{noise}} \quad (24)$$

where $p'_{i,j}(t)$ is the restriction of $p_{i,j}(t)$ to the interval $[uT, vT]$. When the number of nonzero $p'_{i,j}(t)$'s is finite, the optimal $h_{[u,v]}(t)$ can then be constructed as in Section IV-D1. This is illustrated with the Mach–Zehnder example in Section V-B. The resulting filter is a true zero-forcing filter. Otherwise, we can resort to selecting a finite set of $p'_{i,j}(t)$'s as an approximation to the actual lower bound when carrying out the computation. The normalized eye opening, $\frac{1}{M-1}\langle p'_{0,0}, h_{[u,v]}\rangle$, increases with the width of $[uT, vT]$ because one optimizes over a larger set of possible responses. Thus, $\frac{1}{M-1}\langle p'_{0,0}, h_{[u,v]}\rangle$ is a lower bound to the infinite sequence case. The upper and lower bounds approach each other as $n$, $-u$, and $v$ increase.

## V. Applications and Examples

In applying the formulations from Section IV, we consider four examples. The first example considers a Gaussian pulse; the second and third examples involve the use of Mach–Zehnder chain interferometers and Fabry–Perot interferometers for the optical demultiplexing filter; and the fourth example considers long-haul transmission. For these examples, we plot the impulse response and the frequency response of the optimal zero-forcing filter, and eye diagrams for the rectangular and zero-forcing filters. Then we plot the normalized eye opening $\xi$ in dB, i.e., $10\log_{10}(\xi)$, for the matched filter bound, the zero-forcing filter, and the rectangular filter, using two, four, and/or eight level signaling. Note that the normalized eye opening is proportional to the received optical energy.

### A. Gaussian Pulse Example

When we have a Gaussian received optical pulse, $p(t)$, we show that the zero-forcing filter does not exist. Let the received optical pulse be normalized such that $p(t) = e^{-t^2/\sigma^2}$; then

$$p_{i,j}(t) = e^{-(t-iT)^2/\sigma^2 - (t-jT)^2/\sigma^2} \quad (25)$$

and they are positive. When $j = -i$, we have $p_{i,-i}(t) = e^{-2i^2T^2/\sigma^2} p_{0,0}(t)$. The desired product waveform $p_{0,0}(t)$ is proportional to $p_{i,-i}(t)$. Thus, the component of $p_{0,0}(t)$ orthogonal to the ISI space is zero. A zero-forcing filter does not exist for this very peculiar case. Minimum mean square error filters [8] can handle Gaussian pulses.

### B. Mach–Zehnder Chain Interferometer Example

In this example, we consider using a Mach–Zehnder chain interferometer as the optical demultiplexing filter for frequency division multiplexing applications. The Mach–Zehnder chain interferometer is composed of a cascade of Mach–Zehnder interferometers. Let $\Delta L$ be the length difference between the two branches of the Mach–Zehnder interferometer at the first stage. Let the length difference be $2^{i-1}\Delta L$ for the $i$th stage and let $K$ be the number of stages. Further characterization of this interferometer is presented in [11].

The impulse response of the Mach–Zehnder chain interferometer is

$$g_{\text{mz}}(t) = \sum_{i=-M/2+1}^{M/2} \delta\left(t - \frac{(2i-1)}{M}\frac{\Delta L}{\nu}\right) e^{j\frac{K\pi}{2}} \quad (26)$$

where $\nu$ is the speed of propagation in the medium and $M = 2^K$. The corresponding frequency response is

$$G_{\text{mz}}(f) = \frac{\sin\left(M\pi\frac{\Delta L f}{\nu}\right)}{M\sin\left(\pi\frac{\Delta L f}{\nu}\right)} e^{j\frac{K\pi}{2}}. \quad (27)$$

The frequency response $G_{\text{mz}}(f)$ is periodic with the main transmission peaks separated by $\frac{\nu}{\Delta L}$.

We are interested in passing the received optical signal at a transmission peak, say $f_o$, of the demultiplexing filter. The width of frequency interval between $f_o$ and an adjacent peak is equal to $\frac{\nu}{\Delta L}$. Since the filter is a channel selection device, we want the width $\frac{\nu}{\Delta L}$ to cover the system bandwidth, including

all the channels. As the number of channels increases, the width $\frac{\nu}{\Delta L}$ needs also to increase. Let $f' = f - f_o$ be the frequency shifted by $f_o$. For the channel, we are interested where $f$ is close to $f_o$, $|\frac{\Delta L f'}{\nu}| \ll 1$ becomes true as the number of channels increases, and the equivalent baseband channel response is well approximated by $\sin(M\pi\frac{\Delta L f'}{\nu})/(M\pi\frac{\Delta L f'}{\nu})$. We drop a constant phase factor which does not affect the photodetector output.

Note that the frequency response has zeros spaced by $\frac{\nu}{M\Delta L} \equiv \frac{1}{cT}$, where $c = \frac{M\Delta L}{\nu T}$. We will consider only the case $0 \leq c \leq 1$. The zeros in the frequency domain can be used to suppress interchannel interference. In the time domain, the complex envelope of the impulse response is rectangular with height $\frac{1}{cT}$ in the interval $[-\frac{cT}{2}, \frac{cT}{2}]$ and zero otherwise.

We assume that the transmitted pulses are non-return to zero (NRZ). They are simplified versions of pulses used in practice. The complex envelope of the transmitted pulse $g(t)$ is one in the interval $[-\frac{T}{2}, \frac{T}{2}]$ and zero otherwise. The received signal envelope $p(t)$ is trapezoidal with a base extending on $[-(1+c)/2, (1+c)/2]$ and a top extending on $[-(1-c)/2, (1-c)/2]$.

For the upper bound construction, we consider the amplitudes $a_{-n}, \ldots, a_n$, setting the other amplitudes to zero. Due to the finite duration of the received pulse, which is between $T$ and $2T$ for $c$ between zero and one, the nonzero $p_{i,j}(t)$'s are the following:

$$\{p_{i,i}(t) \mid -n \leq i \leq n\} \text{ and } \{p_{i,i-1}(t) \mid -n+1 \leq i \leq n\}. \tag{28}$$

Note that the signal space has dimension $\mathcal{D} = 2$.

For the lower bound construction, we consider the signal space spanned by product waveforms restricted to the interval $[-nT, nT]$. The set of nonzero truncated product waveforms $p'_{i,j}(t)$'s are

$$\{p'_{i,i}(t) \mid -n \leq i \leq n\} \text{ and } \{p'_{i,i-1}(t) \mid -n+1 \leq i \leq n\}. \tag{29}$$

These product waveforms are shown in Fig. 2, where $n = 1$ and $c = \frac{1}{2}$. In Fig. 2(b) the lower bound is for $u = -1$ and $v = 1$. Note that the number of product waveforms that we need to consider is $4n+1$ for the upper and lower bound, and that the product waveforms are nonnegative.

For this example, the bounds show that the optimal filter is well approximated by a finite duration response $h_{[-3T,3T]}(t)$. In Fig. 3, we plot the time and frequency response of $h_{[-3T,3T]}(t)$ when $c = 1$, as well as the resulting eye diagram.

Figure 4 shows the normalized eye openings for the Mach–Zehnder case. The performance of the zero-forcing filter is determined by the bounds in Section IV-D. It is not distinguishable from that of $h_{[-3T,3T]}(t)$.

The zero dB point is the eye opening for the binary case without ISI. The parameter $c' = cTR_b$ is inversely proportional to the optical filter bandwidth (Section V-B) and is proportional to the bit rate $R_b$, i.e., the bandwidth efficiency in units of (b/s/Hz) increases with $c'$. When $c'$ =0, there is no ISI introduced and the vertical offset is due to the scaling factor $\frac{\sqrt{\log_2 M}}{M-1}$ to keep the bit rate and the average energy per bit the same for different $M$. When $c'$ is increased, there is more ISI and the normalized eye opening decreases. The matched filter bound curves also decrease due to the decrease of the electrical pulse energy.

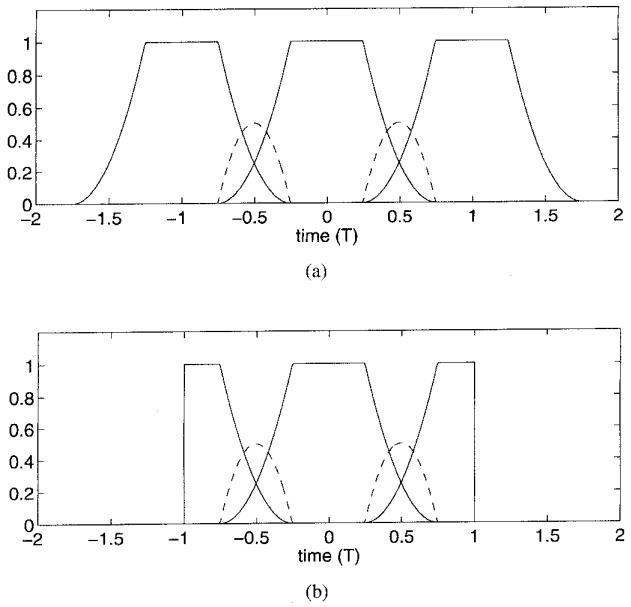


Fig. 2. Product waveforms involved in the upper and lower bounds when $n = 1$. Shown in solid and dashed lines are the product waveforms for (a) the upper bound and (b) the lower bound.

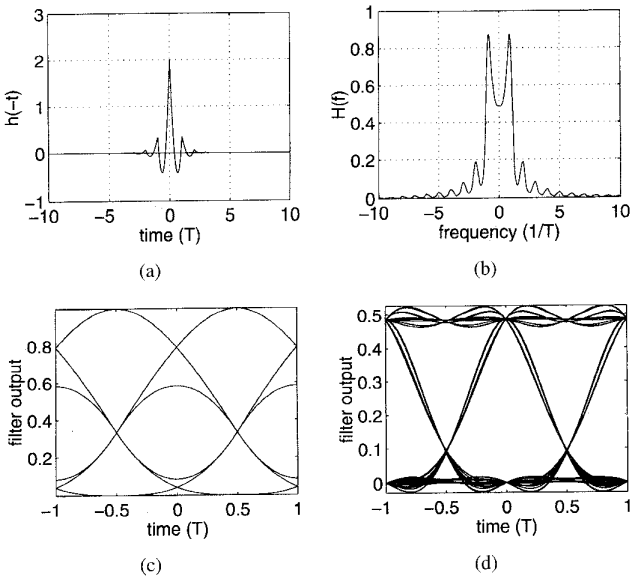


Fig. 3. The optical filter is a Mach-Zehnder interferometer chain. The plots show (a) the impulse response and (b) the frequency response of the zero-forcing filter $h_{[-3T,3T]}(t)$ when $c = 1$. The eye diagrams of the rectangular and zero-forcing filters are shown in plots (c) and (d), respectively.

Figure 4 shows that the zero-forcing filter and the rectangular filter have about the same performance for two-level signaling. For four- and eight-level signaling, the performance difference is more noticeable; the zero-forcing filter has much better performance. For the range of $c'$ that we consider, there is no advantage to four- and eight-level signaling, mainly because the ISI introduced by the optical filter is relatively low.

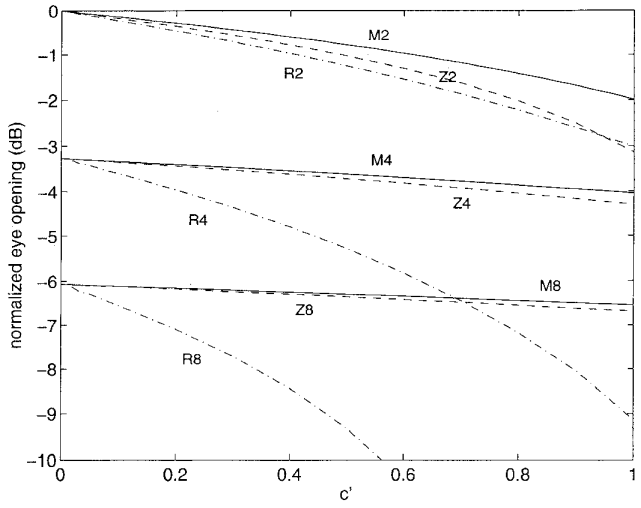


Fig. 4. The optical filter is a Mach–Zehnder interferometer chain.The curves are labeled as follows: $(M)$ matched filter bound, $(Z)$ zero-forcing filter, $(R)$ rectangular filter, and (2, 4, 8)-level signaling.

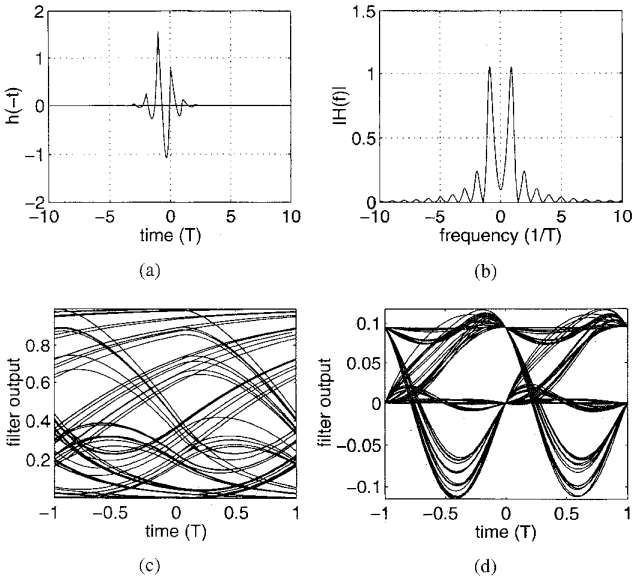


Fig. 5. The optical filter is a Fabry–Perot interferometer. The plots show (a) the impulse response and (b) the magnitude of the frequency response of the zero-forcing filter $h_{[-5T,5T]}(t)$ when $\tau = 1$. The eye diagrams of the rectangular and zero-forcing filters are shown in plots (c) and (d), respectively.

### C. Fabry–Perot Interferometer Example

For this example, the optical demultiplexing filter that we consider is a Fabry–Perot interferometer. This type of interferometers can be implemented on the fiber itself [12]–[14] which allows for compact constructions. More detailed characterization of this interferometer is presented in [11] & [15]. We write the frequency response as

$$G_{\mathrm{FP}}(f) = \frac{1-r^2}{1-r^2e^{-j2\pi f t_d}} \tag{30}$$

where $r$ is the reflection coefficient of each of the mirrors and $t_d$ is the round trip delay of the field between the mirrors.

The frequency response has a peak when $ft_d$ is an integer. We are interested in passing the received optical signal at a transmission peak, say $f_o$, of the demultiplexing filter. The width of frequency interval between $f_o$ and an adjacent peak is equal to $\frac{1}{t_d}$. Let $f' = f - f_o$ be the frequency shifted by $f_o$. Using the argument in the Mach–Zehnder chain interferometer example and for the channel we are interested in where $f$ is close to $f_o$, $|f't_d| \ll 1$ becomes true and the baseband channel response is well approximated by $\frac{1-r^2}{1-r^2(1-j2\pi f' t_d)}$.

The complex envelope of this impulse response is $\frac{1}{\tau T}e^{-t/\tau T}$ for $t \geq 0$, where $\tau T = \frac{t_d R}{1-R}$ and $R = r^2$. Let $B_{\mathrm{FP}}$ be the 3 dB bandwidth of the filter. Then

$$\tau T = \frac{1}{\pi B_{\mathrm{FP}}}.$$

Let the transmitted pulse equal one in the interval $[0, T]$ and zero otherwise. Then the received pulse is

$$p(t) = \begin{cases} 1 - e^{-\frac{t}{\tau T}}, & 0 \leq t < T \\ (e^{1/\tau} - 1)e^{-\frac{t}{\tau T}}, & t \geq T. \end{cases} \tag{31}$$

All $p_{i,j}(t)$'s have the same exponential tail and they are nonnegative. It follows that the $p_{i,j}(t)$'s can be expressed as linear combinations of time-shifted versions of only $p_{0,0}(t)$ and $p_{0,-1}(t)$; thus $\mathcal{D} = 2$. For this example, the optimal filter is well approximated by a finite duration response $h_{[-5T,5T]}(t)$, based on the upper and lower bound considerations in Sections IV-D1 and IV-D2. Fig. 5 shows the impulse and frequency response of $h_{[-5T,5T]}(t)$ when $\tau = 1$, as well as the resulting eye diagram. Note the low DC response of the filter.

Figure 6 shows the normalized eye openings for the Fabry-Perot case. The performance of the zero-forcing filter is determined by the bounds in Section IV-D. It is not distinguishable from that of $h_{[-5T,5T]}(t)$.

The zero dB point is the eye opening for the binary case without ISI. The parameter $\tau' = \tau T R_b$ is inversely proportional to the optical filter bandwidth (Section V-C) and is proportional to the bit rate $R_b$; the bandwidth efficiency in units of (b/s/Hz) increases with $\tau'$.

As $\tau'$ increases, the optical filter bandwidth decreases and there is more ISI. The normalized eye opening closes completely for the rectangular filter case. There is no advantage to four and eight-level signaling for the rectangular filter, the same conclusion as in [15]. On the other hand, the zero-forcing filter performs much better and there is advantage to four-level signaling for large values of $\tau'$.

When ISI is small, having more than two levels of signaling does not provide benefit. When ISI is severe, having four and eight-level signaling provides better normalized eye opening due to a reduction in the baud rate. However, this benefit is achievable only if the design of the receiver can provide sufficient mitigation of the ISI. Enough power should also be available to tolerate the reduced eye opening.

### D. Dispersive Channel Example

One of the impairments that limit data rates and transmission distances is ISI due to fiber dispersion, where the index of refraction of the fiber depends on frequency. Around the

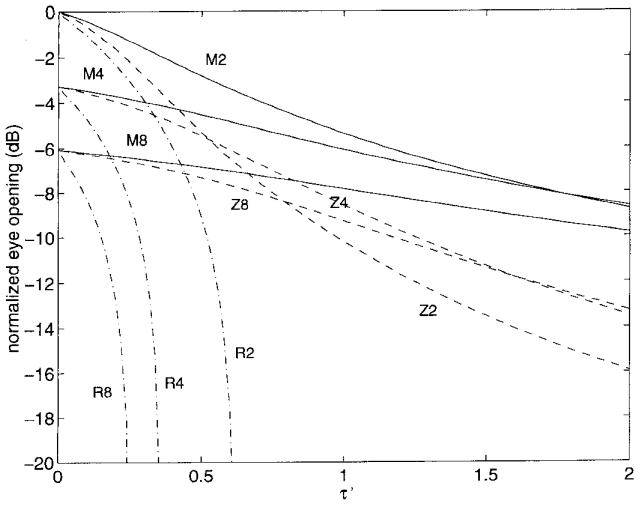


Fig. 6. The optical filter is a Fabry–Perot interferometer. The curves are labeled as follows: $(M)$ matched filter bound, $(Z)$ zero-forcing filter, $(R)$ rectangular filter, and (2, 4, 8)-level signaling.

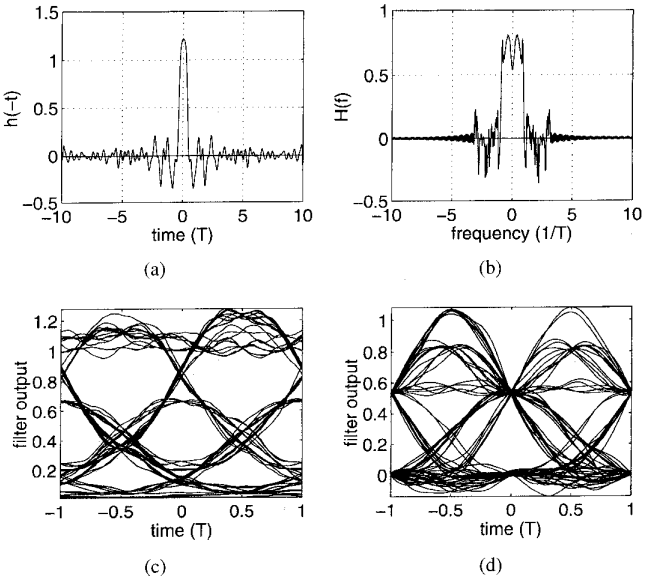


Fig. 7. The dispersive channel case. The plots show (a) the impulse response and (b) the frequency response of the approximated zero-forcing filter $h_{[-10T,10T]}(t)$ when $\alpha = 4$. The eye diagrams of the rectangular and zero-forcing filters are shown in plots (c) and (d), respectively.

center frequency of the transmitted signal, we can expand the phase response of the fiber in terms of a Taylor series. We model the nonlinear phase by keeping the second-order term of the Taylor series expansion and write the response of the dispersive channel as $e^{-j\alpha f^2}$, where $\alpha$ is a scalar given below and $f$ is normalized frequency, i.e., frequency divided by the bit rate. Using normalized frequency allows one to compare systems with different frequency expansion factors in a normalized way.

In the time domain, a transmitted pulse tends to broaden in time as it travels through the transmission medium. The pulse broadening is proportional to the distance that the pulse travels. If we have a fixed distance of transmission, the bit rate has two effects on the severity of ISI. The first effect is that the transmitted pulse duration decreases when the bit rate increases. The spectrum of the pulse becomes wider and the signal is affected more by the nonlinearity of the phase of the medium. Consequently, the relative broadening of the pulse is more severe due to an increase in the data rate. The second effect is that the relative tolerance for pulse broadening decreases when the symbol duration is decreased. Due to these two effects, the severity of ISI increases with the square of the bit rate. These effects on the severity of ISI can be quantified by

$$\alpha = \frac{\pi R_b^2 \lambda^2 D(\lambda) L}{c} \tag{32}$$

where $R_b$ is the bit rate; $\lambda$ is the carrier wavelength; $D(\lambda)$ is the dispersion of the fiber in units of (ps/km·nm); given a one nm bandwidth pulse, one would expect the transmitted pulse to broaden by a certain number of ps after traversing 1 km of the fiber. Note that the parameter $D$ depends on $\lambda$. Continuing with the other parameters, $c$ is the speed of light and $L$ is the length of the fiber.

For conventional fiber, $D$ is about 15 ps/km·nm at $\lambda = 1.5$ $\mu$m. Given the bit rate $R_b = 10^{10}$ bps and the transmission distance $L$ =100 km, we have $\alpha = 3.5$. As another example,

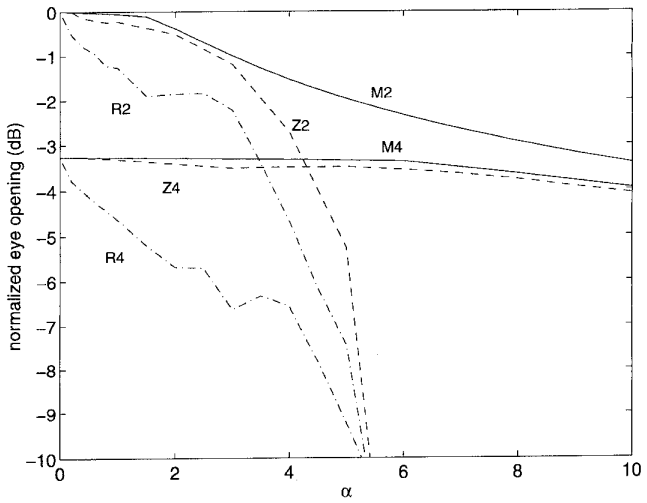


Fig. 8. The dispersive channel case. The curves have the following labels: $(M)$ matched filter bound, $(Z)$ zero-forcing filter, $(R)$ rectangular filter, and (2, 4)-signaling levels.

we decrease the bit rate by a factor of ten and increase the transmission distance by a factor of ten. Then $R_b = 10^9$ bps, $L = 10^3$ km and $\alpha = 0.35$.

The transmitted pulse is a rectangular pulse equal to one for $t$ in $[-\frac{T}{2}, \frac{T}{2}]$ and zero otherwise. In this example, we use the approximated signal space $\tilde{S}_{(0.95)}$. In Fig. 7, we plot the impulse and frequency responses of the approximated zero-forcing filter when $\alpha = 4$, as well as the resulting eye diagram.

Figure 8 shows the normalized eye opening for the dispersive channel case. The performance of the zero-forcing filter is determined by the bounds in Section IV-D. It is not distinguishable from that of $h_{[-10T,10T]}(t)$.

In Fig. 8, the matched filter bound decreases with $\alpha$ because the dispersive channel reduces the electrical energy of the pulse, even though the dispersive channel is all pass in the optical domain. We see that multilevel signaling is advantageous at high bit rates when a zero-forcing filter is used, but not at all with a rectangular filter. However, the length of the equalizer increases with $\alpha$, making the equalizer harder to implement.

## VI. Conclusion

In this paper, we construct minimum noise variance zero-forcing filters for direct detection systems and obtain tight performance bounds. We apply them to practical situations. We find that zero-forcing filters yield better results than rectangular filters in multilevel signaling ($M > 2$) and in severe ISI situations. However, practical implementation of the filters is not considered in this paper and would need further investigation. Important issues are the realization of discrete time filters, the relation between filter performance and the number of taps, and the development of adaptive filters.

## Appendix

In this appendix, we consider phase variations for the transmitted amplitudes. When the transmitted amplitudes are complex, we write the post-detection received signal as

$$r(t) = \left| \sum_{i=-\infty}^{\infty} a_i p(t - iT) \right|^2 + n(t) \tag{33}$$

$$= \sum_{i,j=-\infty}^{\infty} a_i a_j^* p(t - iT) p^*(t - jT) + n(t). \tag{34}$$

The left hand side of the above equation is real, so we can take the real part of the right hand side and write

$$r(t) = \sum_{i,j=-\infty}^{\infty} \mathrm{Re}\{a_i a_j^* p(t - iT) p^*(t - jT)\} + n(t) \tag{35}$$

$$= \sum_{i,j=-\infty}^{\infty} \mathrm{Re}\{a_i a_j^*\} p_{i,j}(t) - \mathrm{Im}\{a_i a_j^*\} q_{i,j}(t) + n(t) \tag{36}$$

where

$$p_{i,j}(t) = \mathrm{Re}\{p(t - iT) p^*(t - jT)\} \tag{37}$$

and

$$q_{i,j}(t) = \mathrm{Im}\{p(t - iT) p^*(t - jT)\}. \tag{38}$$

The waveforms $p_{i,j}(t)$ and $q_{i,j}(t)$ are the real part and the imaginary part of $p(t - iT)p^*(t - jT)$, respectively. We will refer to these waveforms as *product waveforms*. This representation is useful in that we see the post-detection received signal can be represented as a weighted sum of $p_{i,j}(t)$'s and $q_{i,j}(t)$'s. Moreover, we see the simplification in the structure of the signal when any of the following quantities are zero: $\mathrm{Re}\{a_i a_j^*\}$, $\mathrm{Im}\{a_i a_j^*\}$, $p_{i,j}(t)$ and $q_{i,j}(t)$. Note that $\mathrm{Im}\{a_i a_i^*\}$, and $q_{i,i}(t)$ are always zero.

Note that $q_{0,0}(t)$ is zero and the rest of the $q_{i,j}(t)$'s are a part of the ISI space. Adding these product waveforms would tend to contribute to more ISI. However, having phase variation for the transmitted amplitudes is useful in some cases. An example where it is useful is the Mach–Zehnder example, where the set of product waveforms are time-shifted versions of $p_{0,0}(t)$ and $p_{0,1}(t)$. When detecting $p_{0,0}(t)$, the product waveforms $p_{0,1}(t)$ and $p_{0,-1}(t)$ tend to contribute a significant amount of interference. These product waveforms can be set to zero by using the following amplitude set

$$A_k \in \begin{cases} \left\{ \sqrt{\frac{i}{M-1}} \mid 0 \le i \le M-1 \right\} & \text{if } k \text{ is even} \\ \left\{ j\sqrt{\frac{i}{M-1}} \mid 0 \le i \le M-1 \right\} & \text{if } k \text{ is odd.} \end{cases} \tag{39}$$

Then the received signal is composed of weighted sums of $p_{0,0}(t)$ and time-shifted versions of $p_{0,0}(t)$. This provides a significant reduction in the amount of ISI.

For the Fabry–Perot example, (39) is not as useful because the filters still need to be orthogonal to $p_{i,j}(t)$'s that are proportional to $p_{0,1}(t)$ and $p_{0,-1}(t)$. However, we would expect improvement in performance for the Fabry–Perot case when considering the least mean square receivers in [8]. Note also that the $p_{i,j}(t)$'s that are set to zero when using (39) are replaced by the corresponding $q_{i,j}(t)$'s. These $q_{i,j}(t)$'s do not appear in the Fabry–Perot and Mach–Zehnder examples because $p(t)$ is real for these examples. However, the $q_{i,j}(t)$'s do appear in the dispersive channel example when using (39) because $p(t)$ is complex. For the dispersive channel example, we do not expect (39) to be helpful because the amount of interference from $p_{i,j}(t)$'s and $q_{i,j}(t)$'s are about the same.

## References


[1] E. A. Lee and D. G. Messerschmitt, *Digital Communication*. Boston, MA: Kluwer, 1988.

[2] J. H. Winters and R. D. Gitlin, "Electrical signal processing techniques in long-haul fiber-optic systems," *IEEE Trans. Commun.*, vol. 38, no. 9, pp. 1439–1453, Sept. 1990.

[3] J. H. Winters, R. D. Gitlin, and S. Kasturia, "Reducing the effects of transmission impairments in digital fiber optic systems," *IEEE Commun. Mag.*, vol. 31, no. 6, pp. 68–76, June 1993.

[4] J. C. Cartledge, R. G. McKay, and M. C. Nowell, "Performance of smart lightwave receivers with linear equalization," *J. Lightwave Technol.*, vol. 10, no. 8, pp. 1105–1109, Aug. 1992.

[5] M. J. Minardi and M. A. Ingram, "Adaptive crosstalk cancellation in dense wavelength division multiplexing networks," *Electron. Lett.*, vol. 28, no. 17, pp. 1621–1622, Aug. 1992.

[6] D. Marcuse, "Equalization of dispersion in single-mode fibers," *Applied Optics*, vol. 20, no. 4, pp. 696–700, Feb. 1981.

[7] A. J. Anto and D. K. Smith, "Design and characterization of dispersion compensating fiber based on the $lp_{01}$ mode," *J. Lightwave Technol.*, vol. 12, no. 10, pp. 1739–1745, Oct. 1994.

[8] P. C. Li and P. A. Humblet, "LMS electrical filters to reduce intersymbol interference in direct detection optical systems," in *Proc. ICC'94*, New Orleans, LA, May 1994.

[9] P. C. Li, "Direct detection optical systems: intersymbol interference and electrical filter designs," Ph.D. Dissertation, Dept. of EECS, Massachusetts Institute of Technology, Cambridge, MA, 1995.

[10] D. G. Messerschmitt, "A geometric theory of intersymbol interference, part I: Zero-forcing and decision-feedback equalization," *Bell Syst. Tech. J.*, vol. 52, no. 9, pp. 1483–1519, Nov. 1973.

[11] W. M. Hamdy and P. A. Humblet, "Sensitivity analysis of direct detection optical FDMA networks with OOK modulation," *J. Lightwave Technol.*, vol. 11, nos. 5/6, pp. 783–794, May/June 1993.

[12] J. Stone and L. W. Stulz, "Pigtailed high-finesse tunable fiber Fabry–Perot interferometers with large, medium and small free spectral ranges," *Electron. Lett.*, vol. 23, pp. 781–783, 1987.

[13] J. Stone and D. Marcuse, "Ultrahigh finesse fiber Fabry–Perot interferometers," *J. Lightwave Technol.*, vol. LT-4, pp. 382–385, 1986.
[14] J. Stone, "Optical-fiber Fabry–Perot interferometer with finesse of 300," *Electron. Lett.*, vol. 21, no. 11, pp. 504–505, May 1985.
[15] L. J. Cimini and G. J. Foschini, "Can multilevel signaling improve the spectral efficiency of ASK optical FDM systems?" *IEEE Trans. Commun.*, vol. 41, no. 7, pp. 1084–1090, July 1993.

**Peter C. Li** (M'95) received the B.S. degree in electrical engineering from the University of California, Berkeley, in 1987, and the S.M. and Ph.D. degrees in electrical engineering from the Massachusetts Institute of Technology, Cambridge, in 1991 and 1995, respectively.

His research interests include optical communication, high speed transmission systems, and data networks.

Dr. Li is a member of Sigma Xi, Eta Kappa Nu, and Tau Beta Pi.

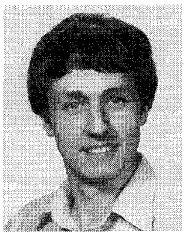

**Pierre A. Humblet** (F'93) received the electrical engineer degree from the University of Louvain, Belgium, in 1973, and the M.S.E.E. and Ph.D. degrees from the Massachusetts Institute of Technology, Cambridge, MA in 1978.

After graduating, he remained at MIT where he became a Professor of Electrical Engineering. In 1993, he joined the Eurecom Institute in France where he heads the Mobile Communications department. His teaching and research interests are in the area of communication systems, particularly mobile, digital, and optical networks.